This is a repository copy of *Extremely low excess noise avalanche photodiode with GaAsSb absorption region and AlGaAsSb avalanche region*.

White Rose Research Online URL for this paper:
https://eprints.whiterose.ac.uk/195921/

Version: Published Version

Article:

Cao, Y. orcid.org/0000-0002-6353-7660, Blain, T. orcid.org/0000-0002-7974-7355, Taylor-Mew, J.D. orcid.org/0000-0002-0895-2968 et al. (3 more authors) (2023) Extremely low excess noise avalanche photodiode with GaAsSb absorption region and AlGaAsSb avalanche region. Applied Physics Letters, 122 (5). ISSN 0003-6951

https://doi.org/10.1063/5.0139495

Reuse
This article is distributed under the terms of the Creative Commons Attribution (CC BY) licence. This licence allows you to distribute, remix, tweak, and build upon the work, even commercially, as long as you credit the authors for the original work. More information and the full terms of the licence here: https://creativecommons.org/licenses/

Takedown
If you consider content in White Rose Research Online to be in breach of UK law, please notify us by emailing eprints@whiterose.ac.uk including the URL of the record and the reason for the withdrawal request.

eprints@whiterose.ac.uk
https://eprints.whiterose.ac.uk/

Applied Physics Letters

Extremely low excess noise avalanche photodiode with GaAsSb absorption region and AlGaAsSb avalanche region

Cite as: Appl. Phys. Lett. **122**, 051103 (2023); https://doi.org/10.1063/5.0139495
Submitted: 20 December 2022 • Accepted: 11 January 2023 • Published Online: 31 January 2023
Published open access through an agreement with JISC Collections

Ye Cao, Tarick Blain, Jonathan D. Taylor-Mew, et al.

COLLECTIONS

This paper was selected as Featured

QBLOX
Integrates all Instrumentation + Software for Control and Readout of **NV-Centers**
visit our website >

© 2023 Author(s).

Extremely low excess noise avalanche photodiode with GaAsSb absorption region and AlGaAsSb avalanche region

Cite as: Appl. Phys. Lett. **122**, 051103 (2023); doi: 10.1063/5.0139495
Submitted: 20 December 2022 · Accepted: 11 January 2023 ·
Published Online: 31 January 2023

Ye Cao, Tarick Blain, Jonathan D. Taylor-Mew, Longyan Li, Jo Shien Ng, and Chee Hing Tan[a)]

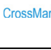

AFFILIATIONS

Department of Electronic and Electric Engineering, The University of Sheffield, Sheffield S1 3JD, United Kingdom

[a)]Author to whom correspondence should be addressed: c.h.tan@sheffield.ac.uk

ABSTRACT

An extremely low noise Separate Absorption and Multiplication Avalanche Photodiode (SAM-APD), consisting of a $GaAs_{0.52}Sb_{0.48}$ absorption region and an $Al_{0.85}Ga_{0.15}As_{0.56}Sb_{0.44}$ avalanche region, is reported. The device incorporated an appropriate doping profile to suppress tunneling current from the absorption region, achieving a large avalanche gain, $\sim$130 at room temperature. It exhibits extremely low excess noise factors of 1.52 and 2.48 at the gain of 10 and 20, respectively. At the gain of 20, our measured excess noise factor of 2.48 is more than three times lower than that in the commercial InGaAs/InP SAM-APD. These results are corroborated by a Simple Monte Carlo simulation. Our results demonstrate the potential of low excess noise performance from $GaAs_{0.52}Sb_{0.48}/Al_{0.85}Ga_{0.15}As_{0.56}Sb_{0.44}$ avalanche photodiodes.

© 2023 Author(s). All article content, except where otherwise noted, is licensed under a Creative Commons Attribution (CC BY) license (http://creativecommons.org/licenses/by/4.0/). https://doi.org/10.1063/5.0139495

Avalanche photodiodes (APDs) are widely used in optical receivers for high-speed optical fiber-based communication and light detection and ranging (LIDAR) at eye-safe wavelengths. When operated in the Geiger mode, they can be used in single photon detection, such as quantum key distribution and quantum imaging. The signal-to-noise ratio (SNR) in an APD-preamplifier module can be enhanced by the internal avalanche gain (M) of APDs if the dominant noise source is the preamplifier. A significant increase in SNR, relative to pin photodiodes, can be achieved if the randomness in the impact ionization process is small. This randomness causes a fluctuation of avalanche gain around a mean value, M, leading to an additional noise, described by the excess noise factor, $F(M)$. The SNR of APDs can be expressed as

$$SNR = \frac{I_{ph}}{2q(I_{ph} + I_d)F(M)B + \sigma^2/M^2},$$

where q is the electron charge, I_{ph} is the photocurrent, I_d is the dark current, B is the bandwidth, and σ^2 is the RMS noise of the amplifier circuit. This equation is appropriate if I_{ph} and I_d are amplified by the same avalanche gain value. The square of the amplifier noise current is reduced by M^2, leading to a significantly increased SNR provided that F increases slowly with M. Therefore, $F(M)$ characteristics are one of the key performance parameters for APDs.

The work from McIntyre shows that $F(M)$ characteristics depend on the semiconductor's ionization coefficients.[1] It is also known that the dead space effect in thin avalanche regions reduces the excess noise factor.[2] The ionization coefficients, denoted by α for electrons and β for holes, are strongly dependent on the electric field and device temperature. To minimize $F(M)$, a semiconductor with a small ionization coefficient ratio, k (α/β if $\beta > \alpha$ or β/α if $\alpha > \beta$) should be chosen, and the ionization process should be dominated by the more readily ionizing carrier type. Si shows extremely low k and is widely used for light detection up to $\sim$900 nm wavelength.[3] For light detection from 1310 to 1550 nm, the $In_{0.53}Ga_{0.47}As$ absorption region is combined with an InP (or $In_{0.52}Al_{0.48}As$) avalanche region in a Separate Absorption and Multiplication Avalanche Photodiodes (SAM-APDs). InP (Ref. 4) and $In_{0.52}Al_{0.48}As$ (Ref. 5) exhibit k approaching unity under high electric fields needed for APD operation; hence, they have worse $F(M)$ characteristics than Si. $AlAs_{0.56}Sb_{0.44}$ (lattice matched to InP substrates) shows extremely low excess noise with effective $k \sim 0.005$ to 0.05 (Refs. 6 and 7) and hence is a promising replacement avalanche material.

More recently, $Al_{0.85}Ga_{0.15}As_{0.56}Sb_{0.44}$ (refer to AlGaAsSb hereafter and lattice matched to InP substrates) exhibits k of 0.05–0.08 in

© Author(s) 2023

170 nm thickness APDs[8] and $F < 2$ for gains up to 25 in a 600 nm thickness APD.[9] A low noise InGaAs/AlGaAsSb SAM-APD has also been reported in Ref. 10. Good excess noise performance was also measured in a 1000 nm AlGaAsSb APD.[11] Similar impressive excess noise data have been reported using AlInAsSb (lattice match to GaSb), with an effective k of 0.01–0.05.[12,13]

We reported a SAM-APD consisting of $GaAs_{0.52}Sb_{0.48}$ (refer to GaAsSb hereafter) absorption region and AlGaAsSb avalanche region grown lattice matched to an InP substrate.[14] The SAM-APD in Ref. 14 exhibited a cutoff wavelength of $\sim$1.7 μm, and an extremely low temperature-coefficient of breakdown voltage, $C_{bd} \sim 4.31 \pm 0.33$ mV/K. However, the doping profile was not sufficiently optimized to suppress band-to-band tunneling current from the GaAsSb absorption region, limiting the usable avalanche gain from the APD performance at high reverse biases. In this paper, we demonstrate a GaAsSb/AlGaAsSb SAM-APD with low tunneling current, high usable avalanche gain, and extremely low excess noise factors.

Compared to the wafer from our previous work,[14] the wafer for this work had increased thickness and doping density for the charge sheet layer. The wafer was grown on a conducting InP (100) substrate by molecular beam epitaxy with Be and Si as the p- and n-type dopants, respectively. An $In_{0.53}Ga_{0.47}As$ layer doped to 5×10^{18} cm^{-3} was grown on the InP substrate as an n^{++} contact layer. The wafer's n^{+} buffer, avalanche, and charge sheet layers were all AlGaAsSb. GaAsSb was used in the absorption, p^{+} buffer, and p^{++} contact layers. Bandgap grading between GaAsSb and AlGaAsSb was implemented using three layers of $Al_{1-x}Ga_xAs_{0.56}Sb_{0.44}$ with Ga composition of 0.2, 0.5, and 0.8. Using standard photolithography techniques and wet chemical etching (with a phosphoric acid-based solution), circular mesa diodes with optical windows were fabricated from the wafer. The diodes' annular top contacts and back contacts were formed by Ti/Au (20/200 nm). The diodes had a radius of 200, 100, 50, or 25 μm. A negative photoresist (SU-8) was used to passivate the mesa sidewalls.

Device characterization was carried out at room temperature, with multiple devices measured for each type of measurement. Current–voltage (I–V) and capacitance–voltage (C–V) characteristics were measured using a Keithley 236 source measure unit and an HP4275 LCR meter, respectively. A 1D Poisson solver was used to fit the experimental C–V characteristics, by adjusting the thickness and doping density of layers from the p^{+} buffer to the n^{+} buffer (a total of six layers). The C–V fitting assumed a built-in voltage of 1.2 V, as well as dielectric constants of 14.04 and 11.41 for GaAsSb and AlGaAsSb, respectively. These dielectric constant values were obtained by linear interpolation using data of AlAs, GaAs, AlSb, and GaSb.[15]

For avalanche gain measurement, light from a modulated 1550 nm wavelength laser was focused on the optical window of the APDs. A lock-in amplifier facilitated phase-sensitive measurement of the photocurrent avoiding the influence of the devices' dark current. A commercial InGaAs photodiode with a known responsivity was used to measure the laser power, yielding responsivity values. Phase-sensitive excess noise measurements were carried out at room temperature using a setup reported in Ref. 16. Optical signals came from a continuous-wave 940 nm wavelength LED that was modulated by a mechanical chopper. Since the 940 nm wavelength light would not be absorbed by the AlGaAsSb charge sheet and avalanche region, a pure electron injection condition was achieved. The excess noise data were obtained from 100 μm radius devices, which have sufficiently large optical windows to avoid unintentional optical injection at the device edges.

Forward and reverse dark I–V data are shown as current density (current normalized to device area) in Fig. 1. Under forward biases, the devices exhibit diode-like characteristics with an ideality factor of 1.8. Under reverse biases, the dark current densities increase abruptly at -48 V. The dark current densities from the three sizes show disagreement up to -48 V, indicating that the surface leakage current dominates before -48 V. Photocurrent density (under the 1550 nm wavelength laser illumination) from a 100 μm radius device is also included in Fig. 1. There is a step increase at -14 V, followed by a gradual increase up to -48 V and finally a steep rise at -48 V. The step increase at -14 V is the punch-through voltage of the APD when the electric field extends to the GaAsSb absorption region and significantly increases the collection efficiency of photogenerated carriers. The punch-through voltage can be observed from the experimental C–V characteristics in Fig. 2, which exhibits a steep decrease in capacitance at -14 V, also plots the C–V fitting (from the 1D Poisson solver), and the associated wafer details. They confirm that the charge sheet in the wafer of this work has a higher doping density and a greater thickness than the previous wafer.[14]

Electric field profiles at selected reverse bias voltages are compared in Fig. 3(a), which also includes those of the previous APD wafer from Ref. 14 for comparison. The previous and current APD wafers with deduced charge sheet layer thicknesses of 62 and 125 nm are now referred to as $APD_{62\,nm}$ and $APD_{125\,nm}$, respectively. $APD_{125\,nm}$ achieves a lower electric field in the GaAsSb absorption region and a higher electric field in the AlGaAsSb avalanche region, suppressing band-to-band tunneling current from the GaAsSb absorption region. At -48 V, the electric field strength in the GaAsSb absorption region is $\sim$250 kV/cm in $APD_{125\,nm}$ compared to 350 kV/cm in $APD_{62\,nm}$. At the same reverse bias, the electric field strength in the avalanche region of $APD_{125\,nm}$ is much higher than that of $APD_{62\,nm}$, ensuring high avalanche gains in $APD_{125\,nm}$.

The higher electric field in the AlGaAsSb region of $APD_{125\,nm}$ could lead to a non-unity gain at a punch-through voltage, which must be accounted for to ensure accurate $M(V)$ and $F(M)$ data.

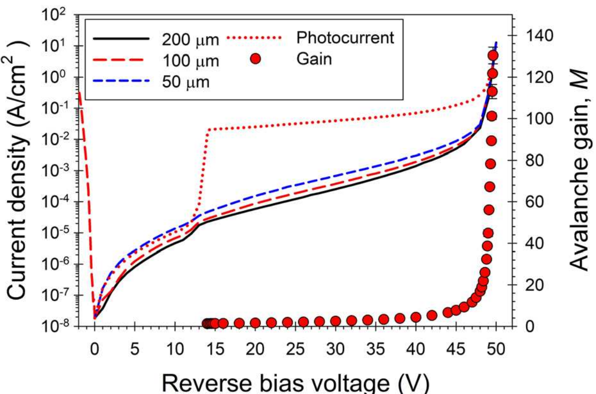

FIG. 1. Room temperature dark current density of 200, 100, and 50 μm radius devices as well as photocurrent density of 100 μm radius device (left axis). Room temperature mean avalanche gain data with standard deviation from six 100 μm radius devices are also shown (right axis).

© Author(s) 2023

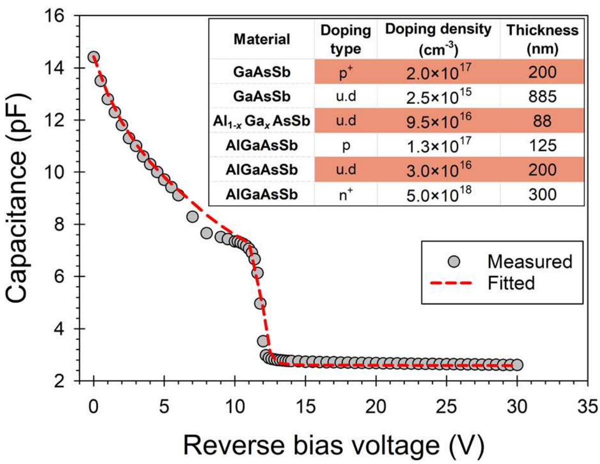

Material	Doping type	Doping density (cm^{-3})	Thickness (nm)
GaAsSb	p^+	2.0×10^{17}	200
GaAsSb	u.d	2.5×10^{15}	885
$Al_{1-x}Ga_xAsSb$	u.d	9.5×10^{16}	88
AlGaAsSb	p	1.3×10^{17}	125
AlGaAsSb	u.d	3.0×10^{16}	200
AlGaAsSb	n^+	5.0×10^{18}	300

FIG. 2. Room temperature measured mean capacitance (from three 100 μm radius devices) and fitting vs reverse bias voltage.

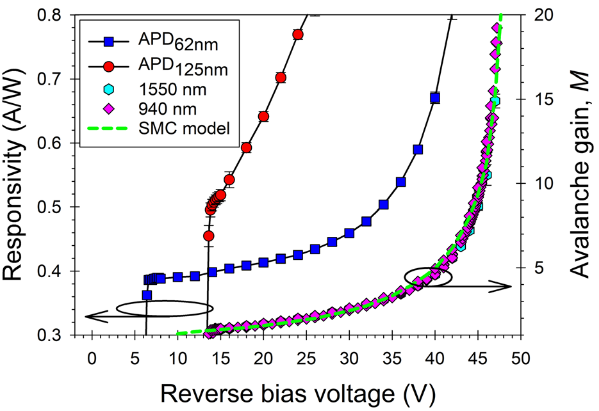

FIG. 4. Mean responsivity at 1550 nm wavelength with standard deviation from $APD_{125\,nm}$ and $APD_{62\,nm}$ (left axis). Avalanche gains for $APD_{125\,nm}$ from multiple devices under 1550 and 940 nm wavelength illumination (right axis). Avalanche gains simulated by the Simple Monte Carlo model (short-dashed line) agree with the experimental results.

To obtain avalanche gain at the punch-through voltage for $APD_{125\,nm}$, responsivity at 1550 nm wavelength was obtained from six devices from each wafer using a fixed optical power of 12 μW. The responsivity data vs reverse bias voltage for both wafers are presented as mean value with standard deviations in Fig. 4. $APD_{62\,nm}$ shows a mean responsivity of 0.386 ± 0.007 A/W at its punch-through voltage of -6.5 V, which remains relatively constant between -6.5 and -10 V, indicating that its gain is unity at -6.5 V. $APD_{125\,nm}$ shows a higher mean responsivity of 0.503 ± 0.009 A/W at -14 V, which continues to increase with voltage, confirming that its gain is non-unity at its punch-through voltage.

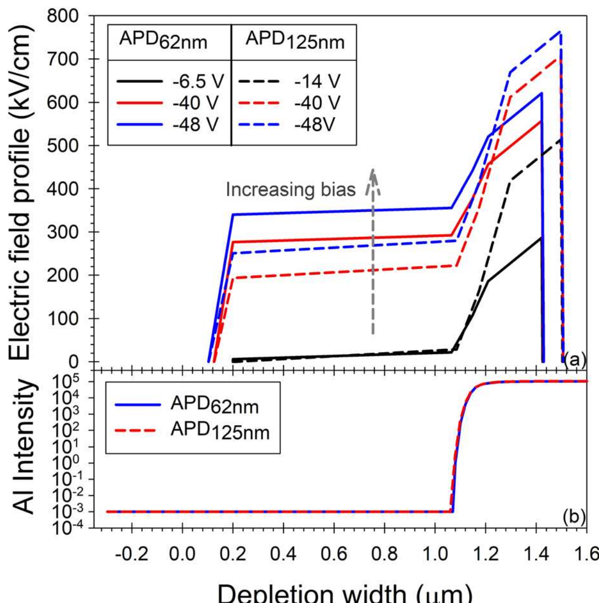

FIG. 3. (a) Estimated electric field profile of $APD_{62\,nm}$ at -6.5 (punch-through voltage), -40, and -48 V, and $APD_{125\,nm}$ at -14 (punch-through voltage), -40, and -48 V; (b) aluminum intensity of $APD_{62\,nm}$ and $APD_{125\,nm}$ from secondary ion mass spectrometry data.

Both wafers have similar absorption region thicknesses, which were confirmed by tracing the aluminum atoms using secondary ion mass spectroscopy, as shown in Fig. 3(b). To understand the differences in the responsivity values in both wafers, we analyzed the electric field profile to determine whether the gain in $APD_{125\,nm}$ is greater than unity at -14 V. From Fig. 3(a), the electric field in the 200 nm thick avalanche region in $APD_{125\,nm}$ varies from 420 to 514 kV/cm at -14 V. From our previous work in Ref. 17, we showed that an avalanche region of 200 nm has a unity gain at the electric field below 300 kV/cm. We have, therefore, used a Simple Monte Carlo (SMC) model that was optimized using an extensive set of experimentally measured gain and excess noise[17] to predict the avalanche gain from the AlGaAsSb charge sheet and the avalanche region in $APD_{125\,nm}$. Using the electric field profile at -14 V from Fig. 3(a), the model predicts a gain of 1.29. In $APD_{62\,nm}$, the peak electric field is 286 kV/cm at –6.5 V, such that it is reasonable to assume its gain is unity. This unity gain reference is corroborated by the unchanged responsivity value shortly after the punch-through voltage at -6.5 V in $APD_{62\,nm}$ in Fig. 4. Hence, the avalanche gain at the punch-through voltage of $APD_{125\,nm}$ is estimated by using the ratio of responsivity values of $APD_{125\,nm}$ to $APD_{62\,nm}$ at a punch-through voltage. This yielded a value of 1.30, which is in excellent agreement with the predicted value, giving us a high confidence level for extracting our avalanche gain values. The gain of 1.30 at -14 V was used to obtain $APD_{125\,nm}$ gain data shown in Fig. 1. $APD_{125\,nm}$ produces a mean gain of $\sim$19 at -48 V and $\sim$130 at -49.6 V.

Having obtained accurate avalanche gain values, we performed the excess noise measurements. The data of avalanche gain from 940 nm wavelength excess noise measurements and 1550 nm wavelength avalanche gain are distinguishable, as shown in Fig. 4 (right axis). This is expected since both wavelengths will produce pure electron injection in this APD. The experimental excess noise factor vs gain characteristics is shown in Fig. 5. Reported excess noise of Si,[3] InGaAs/InP, AlInAsSb,[12] and AlGaAsSb[9,11] are included for

© Author(s) 2023

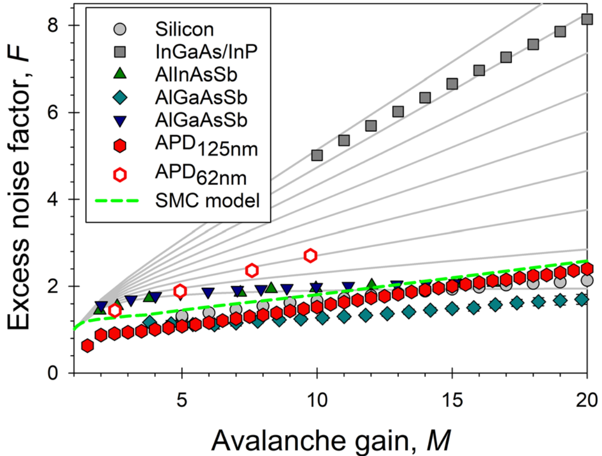

FIG. 5. Comparison of excess noise factor of this work with the reported data for APDs with Si,[3] InGaAs/InP,[18] AlInAsSb,[12] and AlGaAsSb (diamond[9] and triangle down[11]) multiplication region. The mean excess noise factor of $APD_{125\,nm}$ was acquired from eight devices of 100 μm radius. The data points of the mean excess noise factor for $APD_{62\,nm}$ were obtained from six devices of 100 μm radius. SMC predicted excess noise factor vs avalanche gain (short-dashed line) and McIntyre's local model for fixed k value (0–0.4 in a step of 0.05, gray solid lines) are included for comparison.

comparison. The data of this work are comparable to the low excess noise data of Si and AlInAsSb (grown on GaSb) as well as earlier reports of AlGaAsSb.[9,11] Compared to a commercial InGaAs/InP SAM-APD, our GaAsSb/AlGaAsSb SAM-APD data demonstrate significant improvement. For example, at $M = 10$, we obtained $F = 1.52$ compared to $F = 4.8$ in InGaAs/InP SAM-APD. The improvement is more significant at higher gains. At $M = 20$, our APD exhibits $F = 2.48$, which is three times smaller than the 8.0 measured in InGaAs/InP SAM-APD.

The extremely low excess noise performance in $APD_{125\,nm}$ was modeled using the SMC model[19] and the AlGaAsSb SMC model has been validated and the parameter set has been published in Ref. 17. Using the SMC model is essential for this work because of the non-uniform electric field profiles in the AlGaAsSb charge sheet and avalanche region. The simulation uses the deduced electric field profiles in the charge sheet and avalanche region shown in Fig. 3(a). The simulated avalanche gain and excess noise results are in good agreement with the experimental results, as shown in Figs. 4 and 5, respectively.

For completeness, we also measured the excess noise factor in $APD_{62\,nm}$. Due to the presence of band-to-band tunneling current near the breakdown voltage,[14] the excess noise factor was measured up to an avalanche gain of 9.8. To avoid significant overlap with other plots in the graph, we have chosen to plot data at four selected gain values of $M = 2.5$, 4.9, 7.6, and 9.8. The measured excess noise is slightly higher, reaching $F \sim 2.7$ at $M = 9.8$. We attributed this higher excess noise to the onset of avalanche multiplication from the GaAsSb absorption region which has an electric field of more than 300 kV/cm when $M = 3$. At these high fields, the feedback holes from the AlGaAsSb avalanche region could initiate unwanted impact ionization events in the GaAsSb absorption region that led to the increased excess noise factor. A more precise quantification of this will require impact ionization coefficients for GaAsSb, which will be an important future work.

In summary, the optimized charge sheet layer suppressed the tunneling current in the GaAsSb/AlGaAsSb SAM-APD. The surface leakage current is the main source of the dark current, which suggested an improved surface treatment or advanced APD structure is needed. The APD exhibited a high avalanche gain of $\sim$130 at -49.6 V at room temperature and extremely low $F(M)$ of 1.52 at $M = 10$ and $F(M)$ of 2.48 at $M = 20$. The GaAsSb/AlGaAsSb SAM-APD with high avalanche gain and low excess noise showed significant improvement over a commercial InGaAs/InP SAM-APD and offered potential for low photon detection.

This work was supported by the UK-Engineering and Physical Sciences Research Council grants (Nos. EP/N020715/1 and EP/K001469/1). The authors thank the National Epitaxy Facility, at the University of Sheffield, UK, for supplying the wafer. For open access, the author has applied a Creative Commons Attribution (CC BY) license to any Author Accepted Manuscript version arising.

AUTHOR DECLARATIONS

Conflict of Interest

The authors have no conflicts to disclose.

Author Contributions

Ye Cao: Data curation (lead); Formal analysis (lead); Methodology (equal); Validation (equal); Writing – original draft (lead). **Tarick Blain:** Investigation (equal). **Jonathan Derek Taylor-Mew:** Software (equal). **Longyan Li:** Validation (equal). **Jo Shien Ng:** Writing – review & editing (equal). **Chee Hing Tan:** Conceptualization (equal); Formal analysis (equal); Funding acquisition (lead); Investigation (equal); Methodology (equal); Project administration (lead); Resources (lead); Supervision (equal); Writing – original draft (equal); Writing – review & editing (equal).

DATA AVAILABILITY

The data that support the findings of this study are openly available in ORDA, at https://figshare.shef.ac.uk/ [10.15131/shef.data.21753668].

REFERENCES

[1] R. J. McIntyre, IEEE Trans Electron Devices **ED-13**, 164–168 (1966).
[2] M. M. Hayat, B. E. A. Saleh, and M. C. Teich, IEEE Trans. Electron Devices **39**, 546–552 (1992).
[3] HAMAMATSU, *Si APD S10341 Series*, 2017.
[4] L. J. J. Tan, J. S. Ng, C. H. Tan, and J. P. R. David, IEEE J. Quantum Electron. **44**, 378 (2008).
[5] C. H. Tan, Y. L. Goh, A. R. J. Marshall, L. J. J. Tan, J. S. Ng, and J. P. R. David, in *International Conference on Indium Phosphide and Related Materials* (IEEE, 2007), pp. 81–83.
[6] J. Xie, S. Xie, R. C. Tozer, and C. H. Tan, IEEE Trans. Electron Devices **59**, 1 (2012).
[7] X. Yi, S. Xie, B. Liang, L. W. Lim, J. S. Cheong, M. C. Debnath, D. L. Huffaker, C. H. Tan, and J. P. R. David, Nat. Photonics **13**, 683 (2019).
[8] L. L. G. Pinel, S. J. Dimler, X. Zhou, S. Abdullah, S. Zhang, C. H. Tan, and J. S. Ng, Opt. Express **26**, 3568 (2018).
[9] J. Taylor-Mew, V. Shulyak, B. White, C. H. Tan, and J. S. Ng, IEEE Photonics Technol. Lett. **33**, 1155–1158 (2021).
[10] X. Collins, B. White, Y. Cao, T. Osman, J. Taylor-Mew, J. S. Ng, and C. H. Tan, Proc. SPIE **11997**, 1199709 (2022).

© Author(s) 2023

[11]S. Lee, S. H. Kodati, B. Guo, A. H. Jones, M. Schwartz, M. Winslow, C. H. Grein, T. J. Ronningen, J. C. Campbell, and S. Krishna, Appl. Phys. Lett. **118**, 081106 (2021).
[12]M. Ren, S. J. Maddox, M. E. Woodson, Y. Chen, S. R. Bank, and J. C. Campbell, Appl. Phys. Lett. **108**, 10 (2016).
[13]M. Ren, S. J. Maddox, M. E. Woodson, Y. Chen, S. R. Bank, and J. C. Campbell, J. Lightwave Technol. **35**, 2380 (2017).
[14]Y. Cao, T. Osman, E. Clarke, P. K. Patil, J. S. Ng, and C. H. Tan, J. Lightwave Technol. **40**, 4709 (2022).
[15]A. De and C. E. Pryor, Phys. Rev. B **85**, 125201 (2012).
[16]L. Kim Foung, *Avalanche Noise in Submicron GaAs and InP Structures* (Sheffield University, 1999).
[17]J. D. Taylor-Mew, J. D. Petticrew, C. H. Tan, and J. S. Ng, Opt. Express **30**, 17946 (2022).
[18]HAMAMATSU, *InGaAs APD G8931 Series*, 2019.
[19]J. D. Petticrew, S. J. Dimler, and J. S. Ng, J. Open Res. Softw. **6**, 17 (2018).

© Author(s) 2023